


RESEARCH ARTICLE | OCTOBER 21 2024

## Bulk proton conduction in films from a truncated reflectin variant <sup>EP</sup>

Preeta Pratakshya; Albert L. Kwansa; Matic Kovačič; Nikhil Kaimal; Arsenii Panteleev; Atrouli Chatterjee; Nadia E. Tolouei; Rylan Kautz; Kyle L. Naughton; Barbara Sartori; Benedetta Marmiroli; MyAnh K. Dao; Sigrid Bernstorff <sup>ORCID</sup>; Janez Plavec; Yaroslava G. Yingling <sup>ORCID</sup>; Alon A. Gorodetsky <sup>ORCID</sup>  <sup>ORCID</sup>



*APL Mater.* 12, 101113 (2024)  
<https://doi.org/10.1063/5.0214285>



### Articles You May Be Interested In

Proton conduction in inkjet-printed reflectin films

*APL Mater.* (October 2020)

Thermal management of solar thermoelectric power generation

*AIP Conference Proceedings* (July 2022)

Diversity of crabs in the intertidal zone at Sundak Beach, Gunungkidul, Indonesia

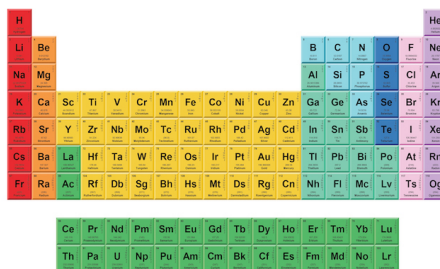
*AIP Conference Proceedings* (August 2018)

30 October 2024 08:35:36



THE MATERIALS SCIENCE MANUFACTURER®

**Now Invent.™**



American Elements  
 Opens a World of Possibilities

...Now Invent!

[www.americanelements.com](http://www.americanelements.com)

© 2021-2024 American Elements & U.S. Registered Trademark

# Bulk proton conduction in films from a truncated reflectin variant

Cite as: APL Mater. 12, 101113 (2024); doi: 10.1063/5.0214285

Submitted: 16 April 2024 • Accepted: 3 June 2024 •

Published Online: 21 October 2024






View Online



Export Citation



CrossMark

Preeta Pratakshya,<sup>1</sup> Albert L. Kwansa,<sup>2</sup> Matic Kovačič,<sup>3</sup> Nikhil Kaimal,<sup>4</sup> Arsenii Pantelev,<sup>4</sup> Atrouli Chatterjee,<sup>4</sup> Nadia E. Tolouei,<sup>4</sup> Rylan Kautz,<sup>5</sup> Kyle L. Naughton,<sup>6</sup> Barbara Sartori,<sup>7</sup> Benedetta Marmiroli,<sup>7</sup> MyAnh K. Dao,<sup>4</sup> Sigrid Bernstorff,<sup>8</sup>  Janez Plavec,<sup>3</sup> Yaroslava G. Yingling,<sup>2</sup>  and Alon A. Gorodetsky<sup>4,5,a)</sup> 

## AFFILIATIONS

<sup>1</sup> Department of Chemistry, University of California, Irvine, Irvine, California 92697, USA

<sup>2</sup> Department of Materials Science and Engineering, North Carolina State University, Raleigh, North Carolina 27695, USA

<sup>3</sup> Slovenian NMR Centre, National Institute of Chemistry, 1000 Ljubljana, Slovenia

<sup>4</sup> Department of Chemical and Biomolecular Engineering, University of California, Irvine, Irvine, California 92697, USA

<sup>5</sup> Department of Materials Science and Engineering, University of California, Irvine, Irvine, California 92697, USA

<sup>6</sup> Department of Physics and Astronomy, University of California, Irvine, Irvine, California 92697, USA

<sup>7</sup> Institute of Inorganic Chemistry, Graz University of Technology, Stremayrgasse 9/IV, 8010 Graz, Austria

<sup>8</sup> Elettra-Sincrotrone Trieste, 34149 Trieste, Italy

<sup>a)</sup> Author to whom correspondence should be addressed: [alon.gorodetsky@uci.edu](mailto:alon.gorodetsky@uci.edu)

## ABSTRACT

Protein- and peptide-based proton-conducting biomaterials have been touted as particularly promising for bioelectronics applications because of their advantageous chemical and physical characteristics, typically excellent biocompatibilities, and readily understood electrical properties. Within this context, our laboratory has previously discovered and systematically investigated bulk proton conduction for a unique family of cephalopod structural proteins called reflectins. Herein, we leverage a combination of experimental and computational methodologies to investigate the bulk electrical properties of hierarchically nanostructured films self-assembled from a previously reported truncated reflectin variant. Our findings indicate that the truncated reflectin variant exhibits protonic conductivities and associated figures of merit on par with those reported for both full-length reflectins and other proteinaceous proton-conducting materials. The combined studies enhance current understanding of reflectins' functional properties within the framework of bioengineering and bioelectronics applications and may ultimately facilitate the development of other protein- and peptide-based conductive biomaterials.

© 2024 Author(s). All article content, except where otherwise noted, is licensed under a Creative Commons Attribution (CC BY) license (<https://creativecommons.org/licenses/by/4.0/>). <https://doi.org/10.1063/5.0214285>

## INTRODUCTION

Protein- and peptide-based proton-conducting biomaterials have been touted as particularly promising for bioelectronics applications because of their numerous advantageous characteristics, including well-defined amino acid sequences, amenabilities to chemical modification, controllable self-assembly properties, straightforward processabilities, and excellent biocompatibilities.<sup>1–6</sup> Within this context, nanostructured films from such biomaterials have generally exhibited excellent electrical properties because of their formation of internal conduits that support effective long-range proton transport.<sup>1–20</sup> For example, bovine serum albumin

(BSA) mats consisting of interconnected fibers have shown proton conductivities of ~0.04 to ~0.3 mS/cm because of proton translocation mediated by the fibers' oxidized amino acids and trapped water molecules.<sup>7,8</sup> In addition, cyclic octapeptide films consisting of self-assembled overlapping nanotubes have featured proton conductivities of ~0.2 to ~0.3 mS/cm because of proton transport mediated by the nanotube octapeptides' side chains and intervening water molecules.<sup>9,10</sup> Moreover, tandem-repeat squid ring teeth protein membranes containing amorphous and crystalline nanoscale domains have possessed proton conductivities of ~0.5 to ~2 mS/cm because of proton hopping through the domains' hydrogen bonded networks.<sup>11,12</sup> Last, hybrid tyrosine-rich peptide films/manganese

oxide composites containing inorganic nanoparticles in peptidic matrices have demonstrated mixed electron–proton conductivities of  $\sim 0.01$  to  $\sim 18.6$  mS/cm in part because of electron transfer-coupled proton migration between oxidized amino acids.<sup>13,14</sup> These and other seminal studies have reinforced the promise and potential of proteinaceous biomaterials for bioelectronics applications while helping establish broadly relevant design guidelines for other biomolecular proton conductors.<sup>7–20</sup>

Within the area of nanostructured protein- and peptide-based biomaterials, our laboratory initially discovered and then systematically investigated bulk proton conduction in unique cephalopod structural proteins called reflectins.<sup>2,21–27</sup> These proteins, which are well known for their critical roles in light-reflecting cephalopod skin cells, possess unusual amino acid sequences that contain multiple conserved repeating domains and feature high aromatic, charged, and polar amino acid contents.<sup>28–35</sup> Due to their unique primary sequences, both reflectins and reflectin-like polypeptides spontaneously self-assemble into spheroidal nanoparticles and can be readily processed into nanostructured thin films under various conditions.<sup>27,29–31,33–36</sup> Such nanostructured films formed from either reflectins or reflectin-like polypeptides exhibit proton conductivities of  $\sim 0.07$  to  $\sim 0.4$  mS/cm at room temperature because of Grotthuss-type proton transport among charged amino acids within hydrophilic nanoscale domains.<sup>21,23,26,27</sup> Accordingly, the reported favorable electrical characteristics have made reflectin variants suitable as active materials for protonic transistors, photochemically dopable platforms, and protochromic devices.<sup>21,22,24,25</sup> Moreover, reflectin-based thin films and nanostructures have exhibited excellent biocompatibilities, as verified by their ability to support human and murine neural stem cell differentiation and their utility as high contrast markers for visualizing or tracking mammalian cells.<sup>37–41</sup> When considered together, the aforementioned studies have suggested that reflectins constitute promising biomaterials for further research and development from the perspective of bioelectronics and bioengineering applications.

Here, we describe proton conduction in nanostructured films self-assembled from a previously reported *Doryteuthis pealeii* reflectin A1 truncated variant (RfA1TV), as illustrated in Fig. 1.<sup>35</sup> Initially, we comparatively investigate the concentration-dependent

structural characteristics of monomeric and self-assembled RfA1TV ensembles in solution, as well as study the morphologies and structural characteristics of nanostructured films fabricated from the self-assembled RfA1TV nanoparticles. Subsequently, we interrogate the electrical properties of our nanostructured RfA1TV films with a combination of alternating current (AC) and direct current (DC) electrical measurements. Finally, we probe the molecular-level arrangements of our monomeric and self-assembled RfA1TV ensembles with both computational and experimental methods. Our findings enhance current understanding of reflectins' reported functional properties and may also help guide the development of other protein- and peptide-based conductive biomaterials.

## RESULTS AND DISCUSSION

We initially comparatively investigated monomeric and self-assembled RfA1TV ensembles in solution. For this purpose, we prepared aqueous solutions containing RfA1TV at low and high concentrations and then characterized them with dynamic light scattering (DLS) and circular dichroism (CD) spectroscopy [see, for example, Fig. 2(a) and the supplementary material for details].<sup>27,34,35,40</sup> For monomeric RfA1TV, the DLS volume distributions revealed a primary peak at typical  $R_H$  values of  $\sim 1$  to  $\sim 2$  nm, which corresponded to a single dominant nanoparticle population [Fig. 2(b)]. The protein's corresponding CD spectra exhibited a main negative peak at  $\sim 200$  nm followed by smaller negative shoulders, indicating a partially ordered secondary structure containing a  $\sim 0.10$  helical fraction and a  $\sim 0.56$  beta structure fraction [Fig. 2(c)]. For self-assembled RfA1TV, the DLS volume distributions revealed peaks at typical  $R_H$  values of  $\sim 10$  to  $\sim 900$  nm, which corresponded to multiple distinct nanoparticle populations [Fig. 2(b)]. The protein's corresponding CD spectra exhibited two negative peaks between  $\sim 203$  and  $\sim 215$  nm, indicating a more ordered secondary structure containing a  $\sim 0.37$  helical fraction and a  $\sim 0.41$  beta structure fraction [Fig. 2(c)]. Notably, the concentration-dependent size distribution and secondary structure trends observed for RfA1TV were similar in water and ammonium formate buffer [compare Figs. 2(b), 2(c), and S1] but were quite different from the previously reported analogous mechanical agitation-dependent

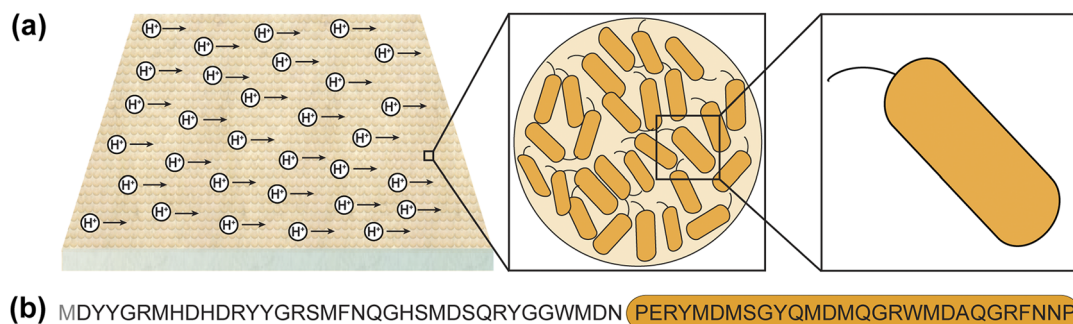


**FIG. 1.** (a) An illustration of a nanostructured film (left) fabricated from self-assembled nanoparticles (middle inset) consisting of a *D. pealeii* reflectin A1 truncated variant (RfA1TV) (right inset). (b) The sequence of RfA1TV, where the conserved motif is denoted by an orange oval.<sup>35</sup> Note that this truncated reflectin variant features an additional N-terminal methionine resulting from bacterial expression.<sup>35</sup>

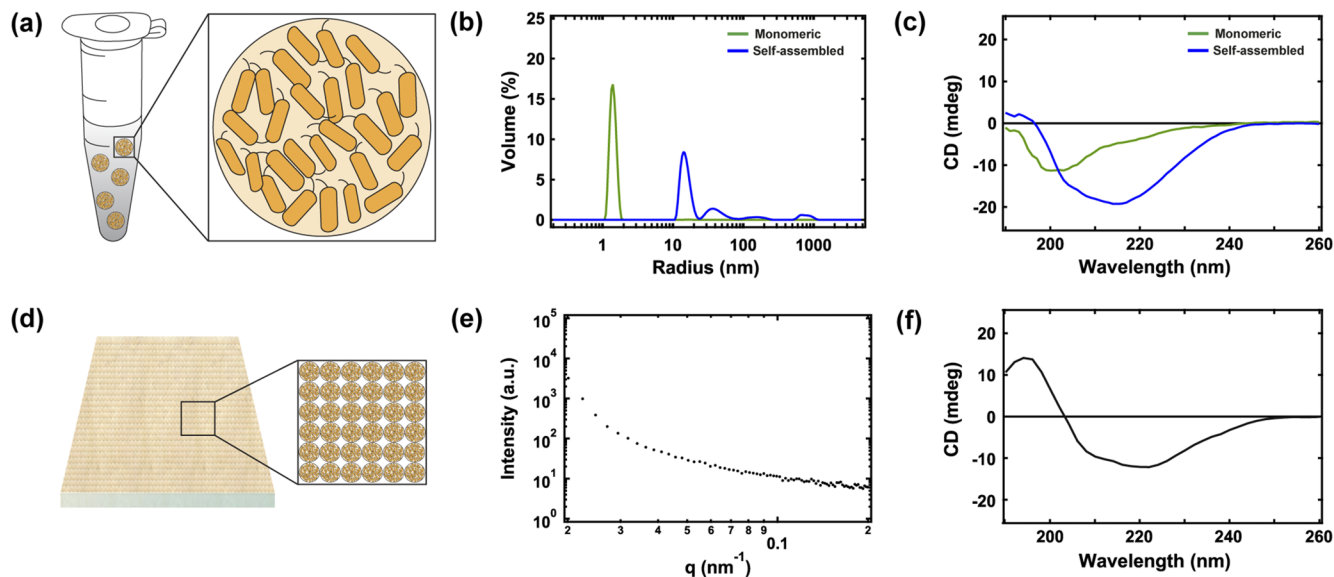


**FIG. 2.** (a) An illustration of nanoparticles self-assembled from RfA1TV. (b) Representative DLS volume distributions obtained for monomeric (green trace) and self-assembled (blue trace) RfA1TV in water. (c) Representative CD spectra obtained for solutions of monomeric (green trace) and self-assembled (blue trace) RfA1TV in water. (d) An illustration of a nanostructured film consisting of RfA1TV nanoparticles. (e) A representative plot of the grazing incidence small-angle x-ray scattering intensity  $I$  as a function of the horizontal scattering vector  $q$  obtained for a nanostructured RfA1TV film. (f) A representative solid-state CD spectrum obtained for a nanostructured RfA1TV film.

trends at low concentrations.<sup>35</sup> These findings provided insight into the evolution of RfA1TV's structural characteristics upon concentration increase-induced self-assembly into nanoparticles in solution.

We next investigated the morphologies of films processed from RfA1TV nanoparticles. For this purpose, we prepared continuous films from high-concentration RfA1TV solutions and then characterized the films with grazing incidence small angle x-ray scattering (GISAXS), atomic force microscopy (AFM), and solid state circular dichroism (ssCD) spectroscopy (note that films prepared from low-concentration RfA1TV solutions were typically discontinuous and, therefore, were challenging to characterize) [see, for example, Fig. 2(d) and the [supplementary material](#) for details].<sup>27,34,35,40</sup> First, the GISAXS scattering intensity data collected and computationally analyzed for the RfA1TV films indicated a radius of gyration ( $R_g$ ) value of  $\sim 170$  nm and a Porod exponent ( $P$ ) of  $\sim 2$ , which were consistent with the presence of large ellipsoidal nanoparticles [Fig. 2(e)]. Second, the AFM imaging performed for continuous RfA1TV films confirmed that their surfaces consisted of coalesced nanoparticles with variable sizes of hundreds of nanometers (Fig. S2). Third, the ssCD spectra obtained for the films revealed a positive peak at  $\sim 195$  nm and two negative peaks at  $\sim 208$  and  $\sim 222$  nm, and therefore, indicated an ordered secondary structure containing a  $\sim 0.43$  helical fraction and a  $\sim 0.35$  beta structure fraction [Fig. 2(f)]. Here, the sizes of the RfA1TV nanoparticles comprising the films were consistent with those of nanoparticles dispersed in solution [Fig. 2(b)] or cast onto solid substrates (Fig. S3). Moreover, the secondary structure of the RfA1TV biomolecules comprising the nanoparticles remained comparable in solution [Fig. 2(c)] and within films [Fig. 2(f)]. These findings showed that self-assembled RfA1TV nanoparticles readily formed films with a distinct nanoscale order and that the

nanoparticles' constituent biomolecules generally maintained their secondary structure in the solid state.

We next interrogated the electrical properties of the RfA1TV films formed from our nanoparticles via alternating current (AC) electrical measurements. Toward this end, we fabricated two-terminal devices consisting of continuous nanostructured RfA1TV films contacted with gold electrodes and characterized such devices with electrochemical impedance spectroscopy (EIS) in the presence of water ( $H_2O$ ) or deuterium oxide ( $D_2O$ ) vapor at a relative humidity (RH) of  $\sim 90\%$  [see, for example, Figs. 3(a), S4, and the [supplementary material](#) for details].<sup>21,23,26,27</sup> The representative Nyquist plots recorded for the RfA1TV-based devices revealed semi-circles and inclined spurs corresponding to bulk film and interfacial film-electrode impedances, respectively, for both  $H_2O$  and  $D_2O$  vapor, as expected for proton-conducting materials [Fig. 3(b)].<sup>2,7,8,21,23,26,27,42,43</sup> The representative Nyquist plots recorded for the RfA1TV-based devices revealed that their average conductivities decreased by  $\sim 34\%$  from  $0.29 \pm 0.08$  to  $0.19 \pm 0.04$  mS/cm upon moving from  $H_2O$  to  $D_2O$ , with this kinetic isotope effect suggesting that proton transport occurred via the Grotthuss mechanism [Fig. 3(b)].<sup>2,5,10,21,23,26,27,44</sup> Here, the Nyquist plots were reasonably modeled with a standard equivalent circuit validated for proton-conducting materials, wherein an RC element represented the bulk film and a constant phase element represented the film-electrode interface (Fig. S5).<sup>21,27,42,43</sup> Moreover, the electrical characteristics and conductivities measured for RfA1TV were similar to those previously reported for full-length reflectins and reflectin-like polypeptides in analogous device configurations under comparable conditions (Table S1).<sup>21,23,26,27</sup> The measurements together indicated that nanostructured RfA1TV films supported proton transport in the solid state.

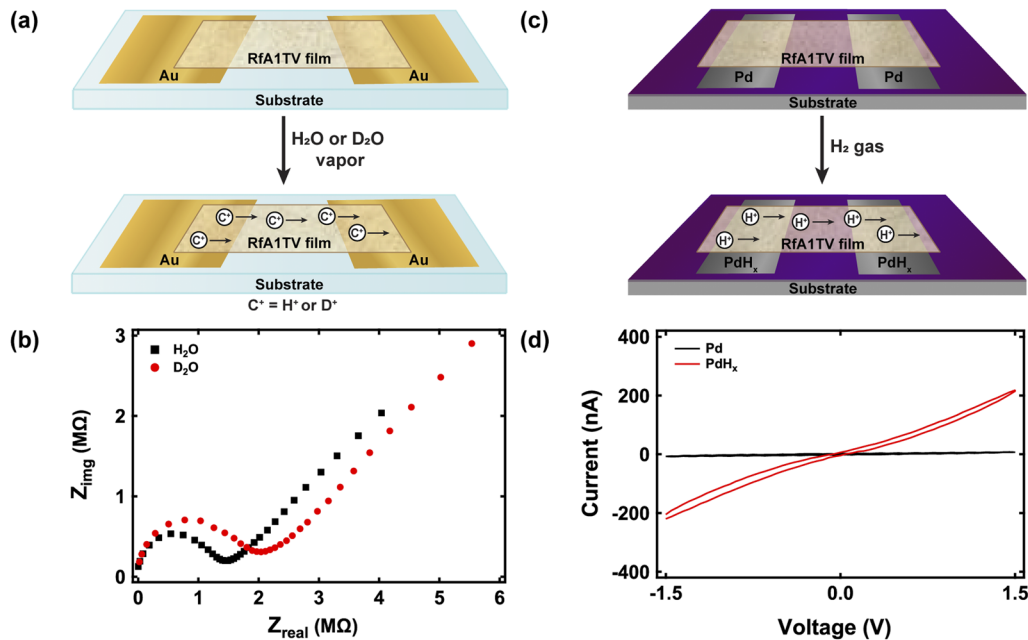


**FIG. 3.** (a) A schematic of an RfA1TV-based two-terminal device contacted with gold electrodes illustrating charge transport in the presence of water ( $\text{H}_2\text{O}$ ) or deuterium oxide ( $\text{D}_2\text{O}$ ) vapor. (b) The Nyquist plots measured for a representative RfA1TV-based two-terminal device contacted with gold electrodes in the presence of  $\text{H}_2\text{O}$  (black squares) and  $\text{D}_2\text{O}$  (red circles) vapor at a RH of  $\sim 90\%$ . (c) A schematic of an RfA1TV-based two-terminal device contacted with palladium (Pd) electrodes illustrating charge transport when the electrodes are converted from Pd to palladium hydride ( $\text{PdH}_x$ ) by exposure to hydrogen ( $\text{H}_2$ ) gas *in situ*. (d) The current as a function of voltage plots measured for a representative RfA1TV-based two-terminal device contacted with Pd (black trace) and  $\text{PdH}_x$  (red trace) electrodes at a RH of  $\sim 90\%$ .

We in turn interrogated the electrical properties of RfA1TV films formed from our nanoparticles via direct current (DC) electrical measurements. Toward this end, we fabricated two-terminal devices consisting of continuous nanostructured RfA1TV films contacted with palladium (Pd) electrodes and characterized the devices via current–voltage (I–V) measurements when the electrodes were converted *in situ* from Pd to palladium hydride ( $\text{PdH}_x$ ) at a RH of  $\sim 90\%$  [see, for example, Figs. 3(c), S6, and the [supplementary material](#) for details].<sup>21–24,26</sup> The representative I–V curves recorded for the RfA1TV-based devices contacted with proton-blocking Pd electrodes revealed slight hysteresis and current densities of  $3.0 \pm 0.3 \text{ mA/cm}^2$  at 1.5 V [Figs. 3(d) and S7]. The representative I–V curves recorded for the RfA1TV-based devices contacted with proton-injecting  $\text{PdH}_x$  electrodes also revealed slight hysteresis but much higher current densities of  $65 \pm 22 \text{ mA/cm}^2$  at 1.5 V [Figs. 3(d) and S7]. Here, the substantial  $\sim 20$ -fold increase in the current densities upon transitioning from proton-blocking to proton-injecting electrical contacts closely matched previous observations for various biomolecular proton-conducting materials [Fig. 3(d)].<sup>13,15–19,21–24,26,45</sup> Moreover, the electrical characteristics and current densities measured for RfA1TV were similar to those previously reported for full-length reflectins in analogous device configurations under comparable conditions (Table S1).<sup>21,23,26</sup> The measurements together confirmed that nanostructured RfA1TV films supported proton transport in the solid state.

We subsequently experimentally probed the molecular-level structure of monomeric and self-assembled RfA1TV *in vitro*. To

achieve this goal, we prepared solutions containing  $^{13}\text{C}$ - and  $^{15}\text{N}$ -labeled RfA1TV at low and high concentrations and then characterized the labeled RfA1TV with two-dimensional (2D) heteronuclear single quantum coherence ( $^1\text{H}$ – $^{15}\text{N}$  HSQC) nuclear magnetic resonance (NMR) spectroscopy [see, for example, Fig. 4(a) and the [supplementary material](#) for details].<sup>35</sup> The  $^1\text{H}$ – $^{15}\text{N}$  HSQC NMR spectra recorded for monomeric and self-assembled RfA1TV revealed different cross-peaks between  $^{15}\text{N}$  chemical shifts of  $\sim 105$  to  $\sim 125$  ppm and  $^1\text{H}$  chemical shifts of  $\sim 7$  to  $\sim 9$  ppm, which could be readily assigned to the individual amino acids [Fig. 4(b)].<sup>35</sup> Here, the chemical shifts recorded for specific amino acids upon RfA1TV's self-assembly into nanoparticles displayed average perturbations  $\Delta\delta(\text{H},\text{N}) = ((\Delta\delta_{\text{H}})^2 + (0.154 * \Delta\delta_{\text{N}})^2)^{1/2}$  with magnitudes as large as  $\sim 0.12$  ppm, indicating a concentration increase-induced rearrangement of the protein's secondary structure [Fig. 4(c)]. Interestingly, the larger chemical shift perturbations found for some charged amino acid residues, e.g., aspartic acid, suggested their participation in local hydrogen bonding or electrostatic interactions within nanoparticles [Figs. 4(a)–4(c)]. Moreover, the pronounced chemical shift perturbations found for RfA1TV's amino acid tracts with a predisposition toward forming alpha helices suggested substantial structural changes and a transition from beta to alpha helical character during self-assembly [Figs. 4(a)–4(c)], in good agreement with our CD observations [Figs. 2(c), 2(f), and S1]. These experiments afforded molecular-level insight into the global ordering that occurred for RfA1TV upon concentration increase-induced self-assembly.



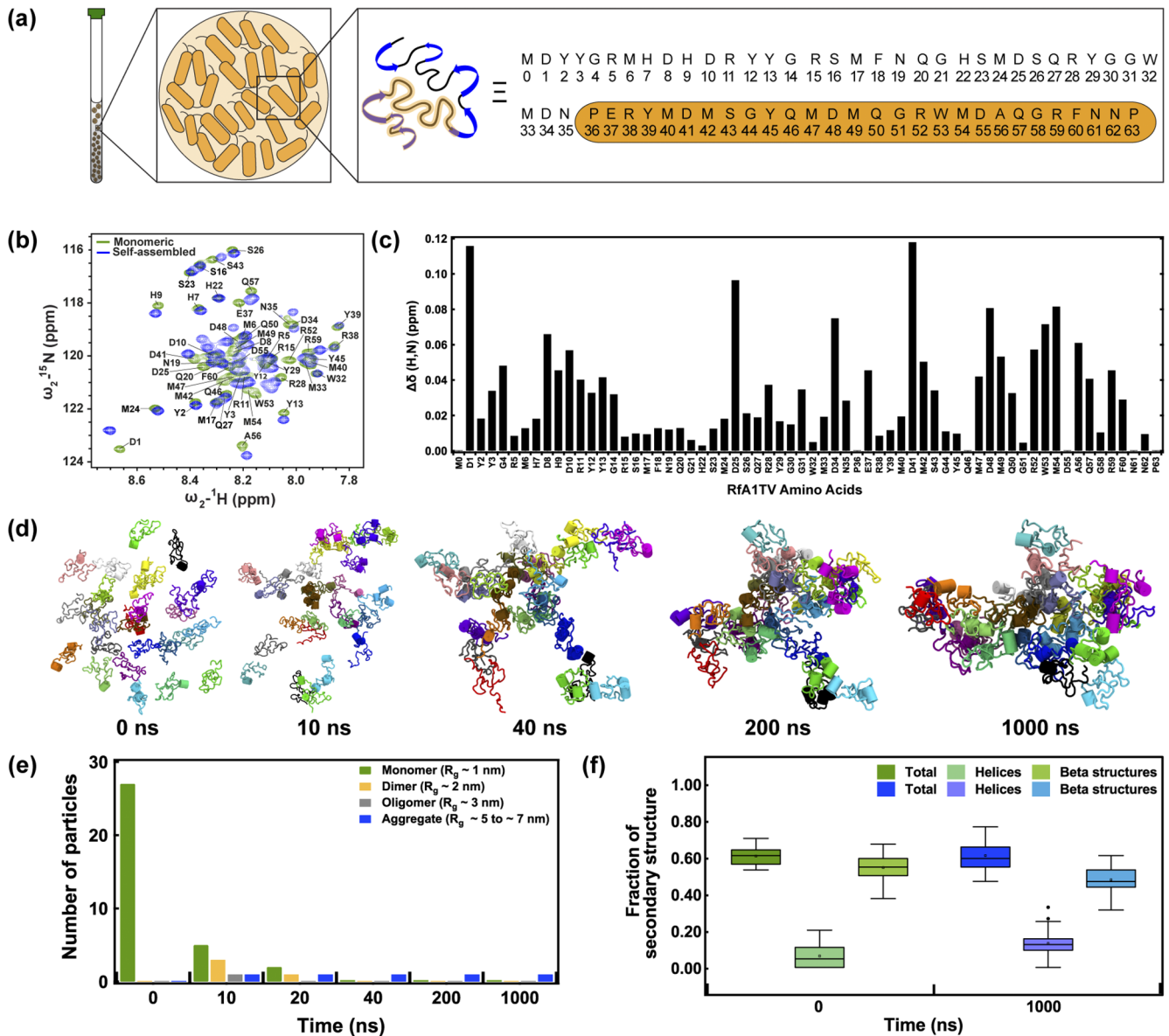


**FIG. 4.** (a) An illustration of self-assembled RfA1TV nanoparticles (left) consisting of RfA1TV monomers (middle inset) that feature the dynamic secondary structural characteristics reported for their amino acid sequence (right inset). (b) A representative  $^1\text{H}$ - $^{15}\text{N}$  HSQC spectrum obtained for monomeric (green peaks) and self-assembled (blue peaks) RfA1TV, where the cross-peaks are labeled with the corresponding numbered amino acids. Note that the signals for the glycine residues are not shown for clarity. (c) A representative bar plot of the chemical shift perturbations  $\Delta\delta(\text{H},\text{N})$  calculated for RfA1TV's amino acids upon self-assembly into nanoparticles. (d) Representative structural snapshots of the RfA1TV ensemble during self-assembly into a nanoparticle. Note that the initial snapshot corresponds to the molecular-level experimental NMR structure reported for RfA1TV.<sup>35</sup> (e) A representative distribution of the number of RfA1TV monomers (green bars), dimers (orange bars), oligomers (gray bars), and aggregates (blue bars) formed during progressive self-assembly of the ensemble into a nanoparticle. (f) Representative box and whisker plots for the total fraction of secondary structure, the fraction of helices, and the fraction of beta structures for a dimeric monomeric RfA1TV ensemble at 0 ns (green boxes) and a self-assembled RfA1TV ensemble at 1000 ns (blue boxes).

We last computationally probed the molecular-level arrangements of monomeric and self-assembled RfA1TV ensembles *in silico*. To achieve this goal, we performed all-atom molecular dynamics (MD) simulations for 27 RfA1TV biomolecules starting

from their experimentally determined monomeric NMR structures and analyzed the evolution of these proteins' aggregation states and secondary structural characteristics [see, for example, Fig. 4(d) and the supplementary material for details].<sup>35,40</sup> The structural

snapshots and particle size distributions calculated for a representative RfA1TV ensemble indicated that the monomeric proteins ( $R_g$  of  $\sim 1$  nm at 0 ns) formed multiple dimers and oligomers ( $R_g$ 's of  $\sim 2$  and  $\sim 3$  nm at 10 ns) before merging into a single large aggregate ( $R_g$  of  $\sim 7$  nm at 40 ns), which subsequently underwent some compaction ( $R_g$  of  $\sim 5$  nm at 200 ns) [Figs. 4(d) and 4(e)]. This multi-stage assembly process appeared driven by the reduction in the total system potential and protein-protein interaction energies for the system (Fig. S8). The structural snapshots and changes in the total fractions of secondary structure calculated for a representative RfA1TV ensemble indicated that the individual proteins generally transitioned from less ordered to more ordered conformations [Figs. 4(d), 4(f), and S9]. This structural transition was evidenced by a notable increase in the fraction of helices (as large as +0.33) and a concomitant decrease in the fraction of beta structures (as large as  $-0.30$ ) for the ensemble [Figs. 4(d), 4(f), and S9], in close overall agreement with our CD and NMR observations [Figs. 2(c), 2(f), Fig. S1, and Figs. 4(b), 4(c)]. These simulations confirmed and reinforced our molecular-level understanding of the structural changes that occurred for RfA1TV ensembles during concentration increase-induced self-assembly.

## CONCLUSION AND SIGNIFICANCE

In summary, we have demonstrated the concentration-dependent self-assembly of RfA1TV into nanoparticles, characterized the morphological and structural characteristics of films fabricated from the RfA1TV nanoparticles, and investigated the electrical properties of such nanostructured RfA1TV films, with our combined observations holding significance for several reasons. First, our synergistic experimental and computational methods consistently indicate that the self-assembled RfA1TV comprising our nanoparticles features altered secondary structures, i.e., shows an increase in the fraction of helices and a corresponding decrease in the fraction of beta structures (relative to monomeric RfA1TV). These findings afford additional insight into RfA1TV's previously predicted ability to sample a broad conformational landscape and thus could ultimately facilitate the improved design of nanostructured reflectin-based optical systems.<sup>35,40,41</sup> Second, the described RfA1TV films processed from the self-assembled nanoparticles exhibit not only global nanoscale-level morphological ordering, i.e., packing of their constituent nanoparticles, but also local molecular-level ordering, i.e., prominent secondary structure changes for some charged amino acids. These findings are consistent with the broader widely reported paradigm that hierarchical multi-length-scale organization promotes effective proton transport in materials derived from either reflectins or other biomolecules,<sup>7–27</sup> thus providing added insight into reflectins' solid state structure-electrical function relationships.<sup>21,34</sup> Third, our nanostructured RfA1TV films surprisingly feature electrical figures of merit, i.e., bulk proton conductivities and associated current densities, which are comparable not only to those reported for full-length reflectins and reflectin-like polypeptides but also to many other proteins or peptides.<sup>7–14,21–27</sup> These findings suggest that our minimal reflectin variant constitutes a promising and tractable template for the design of multifunctional reflectin-inspired conductive biomaterials that could be capable of interfacing with living systems.<sup>2,37,38</sup> Altogether, our findings improve current understanding of reflectins' functional

properties within the framework of bioengineering and bioelectronics applications and may more generally help advance ongoing efforts in the development of protein- and peptide-based conductive biomaterials.

## SUPPLEMENTARY MATERIAL

See the [supplementary material](#) for the detailed experimental procedures, atomic force microscopy images of nanoparticles and films from RfA1TV, optical microscopy images of devices from RfA1TV films contacted with gold and palladium electrodes, computational fits of the electrochemical impedance spectroscopy data obtained for RfA1TV films, expanded views of the current-voltage characteristics obtained for RfA1TV films, the evolution of the total system potential and protein-protein interaction energies for the RfA1TV ensembles, and the changes in the fractions of total secondary structure, helices, and beta structures for the RfA1TV ensembles.

## ACKNOWLEDGMENTS

The authors are grateful to the Air Force Office of Scientific Research (Grant No. FA9550-17-1-0024 to A.A.G.), the Office of Naval Research (Grant No. N00014-20-1-2265 to A.A.G.), and the Army Research Office (Grant No. W911NF-23-1-0052 to Y.G.Y.) for financial support. The authors are grateful to the Slovenian Research and Innovation Agency (Grant No. P1-0242 to J.P.) for financial support. The authors acknowledge the Laser Spectroscopy Labs at the University of California, Irvine, for providing access to experimental facilities. The authors acknowledge the CERIC-ERIC Consortium for access to experimental facilities and financial support. The authors acknowledge North Carolina State University's Office of Information Technology for access to its Henry2 high performance computing cluster.

## AUTHOR DECLARATIONS

### Conflict of Interest

The authors have no conflicts to disclose.

### Author Contributions

A.A.G., J.P., and Y.G.Y. conceived and supervised the project; P.P. and A.C. expressed, purified, and characterized unlabeled RfA1TV; P.P. expressed, purified, and characterized <sup>13</sup>C- and <sup>15</sup>N-labeled RfA1TV; P.P., N.K., and A.P. performed and analyzed the DLS and CD measurements; M.K. performed and analyzed the NMR spectroscopy experiments; A.L.K. performed and analyzed the MD simulations with assistance from A.P.; K.L.N., B.S., B.M., and S.B. performed and analyzed the GISAXS experiments; P.P. fabricated the RfA1TV-based devices contacted with gold electrodes, characterized the devices with optical microscopy and AFM, and performed the EIS experiments and modeling with assistance from N.E.T.; R.K., M.K.D., and P.P. fabricated the RfA1TV-based devices contacted with palladium electrodes, characterized the devices with optical microscopy and AFM, and performed the I-V measurements; A.A.G. and P.P. wrote the paper with input from all of the other co-authors.

**Preeta Pratakshya:** Data curation (lead); Formal analysis (lead); Investigation (lead); Methodology (lead); Visualization (lead); Writing – original draft (lead); Writing – review & editing (equal). **Albert L. Kwansa:** Data curation (equal); Formal analysis (equal); Investigation (equal); Methodology (equal); Visualization (equal); Writing – original draft (equal); Writing – review & editing (equal). **Matic Kovačić:** Data curation (equal); Formal analysis (equal); Investigation (equal); Methodology (equal); Writing – original draft (equal); Writing – review & editing (supporting). **Nikhil Kaimal:** Formal analysis (supporting); Investigation (supporting); Methodology (supporting); Writing – original draft (supporting); Writing – review & editing (equal). **Arsenii Panteleev:** Formal analysis (supporting); Investigation (supporting); Visualization (supporting); Writing – original draft (supporting); Writing – review & editing (equal). **Atrouli Chatterjee:** Investigation (supporting). **Nadia E. Tolouei:** Investigation (supporting). **Rylan Kautz:** Investigation (supporting). **Kyle L. Naughton:** Investigation (supporting). **Barbara Sartori:** Investigation (supporting). **Benedetta Marmioli:** Investigation (supporting). **MyAnh K. Dao:** Investigation (supporting). **Sigrud Bernstorff:** Formal analysis (supporting); Investigation (supporting); Writing – review & editing (supporting). **Janez Plavec:** Conceptualization (equal); Formal analysis (supporting); Funding acquisition (lead); Methodology (supporting); Writing – review & editing (supporting). **Yaroslava G. Yingling:** Conceptualization (equal); Formal analysis (supporting); Funding acquisition (lead); Methodology (supporting); Writing – review & editing (supporting). **Alon A. Gorodetsky:** Conceptualization (lead); Formal analysis (supporting); Funding acquisition (lead); Methodology (supporting); Supervision (lead); Writing – review & editing (equal).

## DATA AVAILABILITY

The data that support the findings of this study are available within the article and its [supplementary material](#) and are available from the corresponding author upon reasonable request.

## REFERENCES

- 1 M. Torculas, J. Medina, W. Xue, and X. Hu, “Protein-based bioelectronics,” *ACS Biomater. Sci. Eng.* **2**, 1211–1223 (2016).
- 2 R. Kautz, D. D. Ordinario, V. Tyagi, P. Patel, T. N. Nguyen, and A. A. Gorodetsky, “Cephalopod-derived biopolymers for ionic and protonic transistors,” *Adv. Mater.* **30**, 1704917 (2018).
- 3 C. D. Bostick, S. Mukhopadhyay, I. Pecht, M. Sheves, D. Cahen, and D. Lederman, “Protein bioelectronics: A review of what we do and do not know,” *Rep. Prog. Phys.* **81**, 026601 (2018).
- 4 N. Amdursky, E. D. Glowacki, and P. Meredith, “Macroscale biomolecular electronics and ionics,” *Adv. Mater.* **31**, 1802221 (2019).
- 5 M. Jia, J. Kim, T. Nguyen, T. Duong, and M. Rolandi, “Natural biopolymers as proton conductors in bioelectronics,” *Biopolymers* **112**, e23433 (2021).
- 6 M. Chen, X. Fu, Z. Chen, J. Liu, and W. Zhong, “Protein-engineered functional materials for bioelectronics,” *Adv. Funct. Mater.* **31**, 2006744 (2021).
- 7 N. Amdursky, X. Wang, P. Meredith, D. D. C. Bradley, and M. M. Stevens, “Long-range proton conduction across free-standing serum albumin mats,” *Adv. Mater.* **28**, 2692–2698 (2016).
- 8 Y. Agam, R. Nandi, T. Bulava, and N. Amdursky, “The role of the protein–water interface in dictating proton conduction across protein-based biopolymers,” *Mater. Adv.* **2**, 1739–1746 (2021).
- 9 S. Roy, L. Zheng, O. Silberbush, M. Engel, Y. Atsmon-Raz, Y. Miller, A. Migliore, D. N. Beratan, and N. Ashkenasy, “Mechanism of side chain-controlled proton conductivity in bioinspired peptidic nanostructures,” *J. Phys. Chem. B* **125**, 12741–12752 (2021).
- 10 O. Silberbush, M. Engel, I. Sivron, S. Roy, and N. Ashkenasy, “Self-assembled peptide nanotube films with high proton conductivity,” *J. Phys. Chem. B* **123**, 9882–9888 (2019).
- 11 A. Pena-Francesch, H. Jung, M. A. Hickner, M. Tyagi, B. D. Allen, and M. C. Demirel, “Programmable proton conduction in stretchable and self-healing proteins,” *Chem. Mater.* **30**, 898–905 (2018).
- 12 Y. Kikuchi, A. Pena-Francesch, M. Vural, and M. C. Demirel, “Highly conductive self-healing biocomposites based on protein mediated self-assembly of PEDOT:PSS films,” *ACS Appl. Bio Mater.* **3**, 2507–2515 (2020).
- 13 J. Lee, I. R. Choe, Y. Kim, S. D. Namgung, K. Jin, H. Ahn, T. Sung, J. Kwon, Y. Lee, and K. T. Nam, “Proton conduction in a tyrosine-rich peptide/manganese oxide hybrid nanofilm,” *Adv. Funct. Mater.* **27**, 1702185 (2017).
- 14 M. Ju, O. H. Cho, J. Lee, S. D. Namgung, M. Song, M. Balamurugan, J. Kwon, and K. T. Nam, “Quantitative analysis of the coupling between proton and electron transport in peptide/manganese oxide hybrid films,” *Phys. Chem. Chem. Phys.* **22**, 7537–7545 (2020).
- 15 C. Zhong, Y. Deng, A. F. Roudsari, A. Kapetanovic, M. P. Anantram, and M. Rolandi, “A polysaccharide bioprotonic field-effect transistor,” *Nat. Commun.* **2**, 476 (2011).
- 16 Y. Deng, E. Josberger, J. Jin, A. F. Roudsari, B. A. Helms, C. Zhong, M. P. Anantram, and M. Rolandi, “H<sup>+</sup>-type and OH<sup>-</sup>-type biological protonic semiconductors and complementary devices,” *Sci. Rep.* **3**, 2481 (2013).
- 17 J. Wunsche, Y. Deng, P. Kumar, E. Di Mauro, E. Josberger, J. Sayago, A. Pezzella, F. Soavi, F. Cicoira, M. Rolandi, and C. Santato, “Protonic and electronic transport in hydrated thin films of the pigment eumelanin,” *Chem. Mater.* **27**, 436–442 (2015).
- 18 S. M. M. Reddy, E. Rablenberg, S. Sloan-Dennison, T. Hesketh, O. Silberbush, T. Tuttle, E. Smith, D. Graham, K. Faulds, R. V. Ulijn, N. Ashkenasy, and A. Lampel, “Proton-conductive melanin-like fibers through enzymatic oxidation of a self-assembling peptide,” *Adv. Mater.* **32**, 2003511 (2020).
- 19 E. E. Josberger, P. Hassanzadeh, Y. Deng, J. Sohn, M. J. Rego, C. T. Amemiya, and M. Rolandi, “Proton conductivity in ampullae of Lorenzini jelly,” *Sci. Adv.* **2**, e1600112 (2016).
- 20 M. Phillips, A. C. Wheeler, M. J. Robinson, V. Leppert, M. Jia, M. Rolandi, L. S. Hirst, and T. Amemiya, “Colloidal structure and proton conductivity of the gel within the electrosensory organs of cartilaginous fishes,” *iScience* **24**, 102947 (2021).
- 21 D. D. Ordinario, L. Phan, W. G. Walkup IV, J.-M. Jocson, E. Karshlev, N. Hüskens, and A. A. Gorodetsky, “Bulk protonic conductivity in a cephalopod structural protein,” *Nat. Chem.* **6**, 596–602 (2014).
- 22 D. D. Ordinario, L. Phan, J.-M. Jocson, T. Nguyen, and A. A. Gorodetsky, “Protonic transistors from thin reflectin films,” *APL Mater.* **3**, 014907 (2015).
- 23 D. D. Ordinario, L. Phan, W. G. Walkup IV, Y. Van Dyke, E. M. Leung, M. Nguyen, A. G. Smith, J. Kerr, M. Naeim, I. Kymissis, and A. A. Gorodetsky, “Production and electrical characterization of the reflectin A2 isoform from *Doryteuthis (Loligo) pealeii*,” *RSC Adv.* **6**, 57103–57107 (2016).
- 24 D. D. Ordinario, L. Phan, Y. Van Dyke, T. Nguyen, A. G. Smith, M. Nguyen, N. M. Mofid, M. K. Dao, and A. A. Gorodetsky, “Photochemical doping of protonic transistors from a cephalopod protein,” *Chem. Mater.* **28**, 3703–3710 (2016).
- 25 D. D. Ordinario, E. M. Leung, L. Phan, R. Kautz, W. K. Lee, M. Naeim, J. P. Kerr, M. J. Aquino, P. E. Sheehan, and A. A. Gorodetsky, “Protochromic devices from a cephalopod structural protein,” *Adv. Opt. Mater.* **5**, 1600751 (2017).
- 26 Y. Lu, P. Pratakshya, A. Chatterjee, X. Jia, D. D. Ordinario, L. Phan, J. A. Cerna Sanchez, R. Kautz, V. Tyagi, P. Patel, Y. Van Dyke, M. K. Dao, J. P. Kerr, J. Long, A. Allevato, J. Leal-Cruz, E. Tseng, E. R. Peng, A. Reuter, J. Couvrette, S. Drake, F. G. Omenetto, and A. A. Gorodetsky, “Proton conduction in inkjet-printed reflectin films,” *APL Mater.* **8**, 101113 (2020).
- 27 C. Xu, N. Kandel, X. Qiao, M. I. Khan, P. Pratakshya, N. E. Tolouei, B. Chen, and A. A. Gorodetsky, “Long-range proton transport in films from a reflectin-derived polypeptide,” *ACS Appl. Mater. Interfaces* **13**, 20938–20946 (2021).



- <sup>28</sup>W. J. Crookes, L. L. Ding, Q. L. Huang, J. R. Kimbell, J. Horwitz, and M. J. McFall-Ngai, "Reflectins: The unusual proteins of squid reflective tissues," *Science* **303**, 235–238 (2004).
- <sup>29</sup>R. M. Kramer, W. J. Crookes-Goodson, and R. R. Naik, "The self-organizing properties of squid reflectin protein," *Nat. Mater.* **6**, 533–538 (2007).
- <sup>30</sup>G. Qin, P. B. Dennis, Y. Zhang, X. Hu, J. E. Bressner, Z. Sun, W. J. Crookes-Goodson, R. R. Naik, F. G. Omenetto, and D. L. Kaplan, "Recombinant reflectin-based optical materials," *J. Polym. Sci., Part B: Polym. Phys.* **51**, 254–264 (2013).
- <sup>31</sup>R. Levenson, C. Bracken, N. Bush, and D. E. Morse, "Cyclable condensation and hierarchical assembly of metastable reflectin proteins, the drivers of tunable biophotonics," *J. Biol. Chem.* **291**, 4058–4068 (2016).
- <sup>32</sup>R. Levenson, D. G. DeMartini, and D. E. Morse, "Molecular mechanism of reflectin's tunable biophotonic control: Opportunities and limitations for new optoelectronics," *APL Mater.* **5**, 104801 (2017).
- <sup>33</sup>A. Chatterjee, B. Norton-Baker, L. E. Bagge, P. Patel, and A. A. Gorodetsky, "An introduction to color-changing systems from the cephalopod protein reflectin," *Bioinspir. Biomim.* **13**, 045001 (2018).
- <sup>34</sup>K. L. Naughton, L. Phan, E. M. Leung, R. Kautz, Q. Lin, Y. Van Dyke, B. Marmioli, B. Sartori, A. Arvai, S. Li, M. E. Pique, M. Naeim, J. P. Kerr, M. J. Aquino, V. A. Roberts, E. D. Getzoff, C. Zhu, S. Bernstorff, and A. A. Gorodetsky, "Self-assembly of the cephalopod protein reflectin," *Adv. Mater.* **28**, 8405–8412 (2016).
- <sup>35</sup>M. J. Umerani, P. Pratakshya, A. Chatterjee, J. A. Cerna Sanchez, H. S. Kim, G. Ilc, M. Kovačić, C. Magnan, B. Marmioli, B. Sartori, A. L. Kwansa, H. Orins, A. W. Bartlett, E. M. Leung, Z. Feng, K. L. Naughton, B. Norton-Baker, L. Phan, J. Long, A. Allevalo, J. E. Leal-Cruz, Q. Lin, P. Baldi, S. Bernstorff, J. Plavec, Y. G. Yingling, and A. A. Gorodetsky, "Structure, self-assembly, and properties of a truncated reflectin variant," *Proc. Natl. Acad. Sci. U. S. A.* **117**, 32891–32901 (2020).
- <sup>36</sup>T. Cai, K. Han, P. Yang, Z. Zhu, M. Jiang, Y. Huang, and C. Xie, "Reconstruction of dynamic and reversible color change using reflectin protein," *Sci. Rep.* **9**, 5201 (2019).
- <sup>37</sup>L. Phan, R. Kautz, J. Arulmoli, I. H. Kim, D. T. T. Le, M. A. Shenk, M. M. Pathak, L. A. Flanagan, F. Tombola, and A. A. Gorodetsky, "Reflectin as a material for neural stem cell growth," *ACS Appl. Mater. Interfaces* **8**, 278–284 (2016).
- <sup>38</sup>R. Kautz, L. Phan, J. Arulmoli, A. Chatterjee, J. P. Kerr, M. Naeim, J. Long, A. Allevalo, J. E. Leal-Cruz, L. Le, P. Derakhshan, F. Tombola, L. A. Flanagan, and A. A. Gorodetsky, "Growth and spatial control of murine neural stem cells on reflectin films," *ACS Biomater. Sci. Eng.* **6**, 1311–1320 (2020).
- <sup>39</sup>A. Chatterjee, J. A. Cerna Sanchez, T. Yamauchi, V. Taupin, J. Couvrette, and A. A. Gorodetsky, "Cephalopod-inspired optical engineering of human cells," *Nat. Commun.* **11**, 2708 (2020).
- <sup>40</sup>A. Chatterjee, P. Pratakshya, A. L. Kwansa, N. Kaimal, A. H. Cannon, B. Sartori, B. Marmioli, H. Orins, Z. Feng, S. Drake, J. Couvrette, L. Le, S. Bernstorff, Y. G. Yingling, and A. A. Gorodetsky, "Squid skin cell-inspired refractive index mapping of cells, vesicles, and nanostructures," *ACS Biomater. Sci. Eng.* **9**, 978–990 (2023).
- <sup>41</sup>G. Bogdanov, A. Chatterjee, N. Makeeva, A. Farrukh, and A. A. Gorodetsky, "Squid leucophore-inspired engineering of optically dynamic human cells," *iScience* **26**, 106854 (2023).
- <sup>42</sup>T. Soboleva, Z. Xie, Z. Shi, E. Tsang, T. Navessin, and S. Holdcroft, "Investigation of the through-plane impedance technique for evaluation of anisotropy of proton conducting polymer membranes," *J. Electroanal. Chem.* **622**, 145–152 (2008).
- <sup>43</sup>A. J. Bard and L. R. Faulkner, *Electrochemical Methods: Fundamentals and Applications*, 2nd ed. (Wiley, 2000).
- <sup>44</sup>N. Agmon, "The Grotthuss mechanism," *Chem. Phys. Lett.* **244**, 456–462 (1995).
- <sup>45</sup>M. Amit, S. Roy, Y. Deng, E. Josberger, M. Rolandi, and N. Ashkenasy, "Measuring proton currents of bioinspired materials with metallic contacts," *ACS Appl. Mater. Interfaces* **10**, 1933–1938 (2018).